



PAPER

Effect of post-process and in-process cooling on wide-area stir zone processed via friction stir processing with pin overlapping

To cite this article: B V S Keerthana *et al* 2023 *Eng. Res. Express* **5** 025060

View the [article online](#) for updates and enhancements.

You may also like

- [Microstructural and tribological properties of A356 based surface hybrid composite produced by friction stir processing](#)
A H Adibpour, I Ebrahimzadeh and F Gharavi
- [Effect of multi-pass friction stir processing on microstructure and mechanical properties of cast Al-7Fe-5Ni alloy](#)
Mojtaba Fekri Soustani, Reza Taghiabadi, Mostafa Jafarzagdegan *et al.*
- [Mechanical and wear behaviour of Friction stir processed surface composite through Self-Assembled Monolayer Technique](#)
Ravi Butola, Ranganath M Singari and Qasim Murtaza

Engineering Research Express



PAPER

Effect of post-process and in-process cooling on wide-area stir zone processed via friction stir processing with pin overlapping

RECEIVED
29 October 2022

REVISED
28 May 2023

ACCEPTED FOR PUBLICATION
2 June 2023

PUBLISHED
12 June 2023

B V S Keerthana^{1,*} , M V N V Satyanarayana², K Venkateswara Reddy³ and M N S Shankar¹

¹ Visvesvarayya Technological University, Belgaum, Karnataka, India

² Anil Neerukonda Institute of Technology and Sciences, Visakhapatnam, Andhra Pradesh, India

³ Marri Laxman Reddy Institute of Technology and Management, Hyderabad, India

* Author to whom any correspondence should be addressed.

E-mail: keerthanaphd23@gmail.com

Keywords: post-process friction stir processing, in-process friction stir processing, overlapping technique, wide-area stir zone, mechanical properties, electrochemical behavior

Abstract

In the current investigation, the influence of post-process and in-process cooling on microstructural, mechanical and electrochemical behavior of wide-area stir zone (WSZ) processed with overlapping friction stir processing (OL-FSP) was studied. The WSZ was successfully prepared in Al5083 aluminum alloy using multi-pass friction stir processing (FSP) with 50% pin overlapping under both cooling conditions. The post-process cooling FSP (PP-FSP) used solid CO₂ as cooling media, whereas the in-process cooling FSP (IP-FSP) used water as cooling media. The microstructural investigations revealed that grain refinement is uniform in each overlapping pass for both cooling conditions. The IP-FSP resulted in better grain refinement than PP-FSP. Three different types of intermetallic particles (needle-shaped Fe-containing, rod-shaped Mg-containing, and very small Mg-containing grain boundary intermetallic particles) were identified in the base alloy and OL-FSP samples. The hardness was observed to be constant across the WSZ due to the uniform grain refinement, and the IP-FSP sample has better hardness and strength than the PP-FSP sample due to the better cooling effect. The elongation followed a similar trend of hardness. The electrochemical findings revealed that the IP-FSP sample has better corrosion resistance than the PP-FSP sample due to the better grain refinement and fine intermetallics.

1. Introduction

A thermo-mechanical process known as friction stir processing (FSP) had outstanding achievements in attaining grain refining in metals and alloys, and it was discovered by Rajeev S Mishra using the friction stir welding (FSW) operating principles. In the initial days, FSP has been used to repair the defective regions. The use then expanded in order to achieve the grain refining, fabricate the composite structures in aluminum alloys, and alter the morphology of relatively thin layers for characteristic improvement [1]. The working methodology of the friction stir processing is extremely simple and same to the operating principles of friction stir welding. To stop metal from running out of the probe region, a revolving tool made up of a shoulder and probe plunges the work material till the shoulder accomplishes a slight plunging with the working plate [2]. To acquire the correct plastic flow behavior, the tool constantly revolves at the penetrated location in the working plate; after the appropriate plasticity is attained, the tool begins to move over the path of action. The distorted material is transported around the probe throughout the tool travel from the advancing side (AS) to the retreating side (RS), where it is deposited [3]. Usually, the tool is tilted downwards between 0.5 and 3.5 degrees so that the distal end of the shoulder forges deformed material and consolidates behind it [4].

It is well known that frictional heat is generated between the work and tool junction, and the stirring action of the tool refines the grains [5]. Once the tool leaves the processed region, the frictional heat that exists in the process leads to the grain growth of recrystallized fine grains. Hence, the desired refinement is not achieved. In

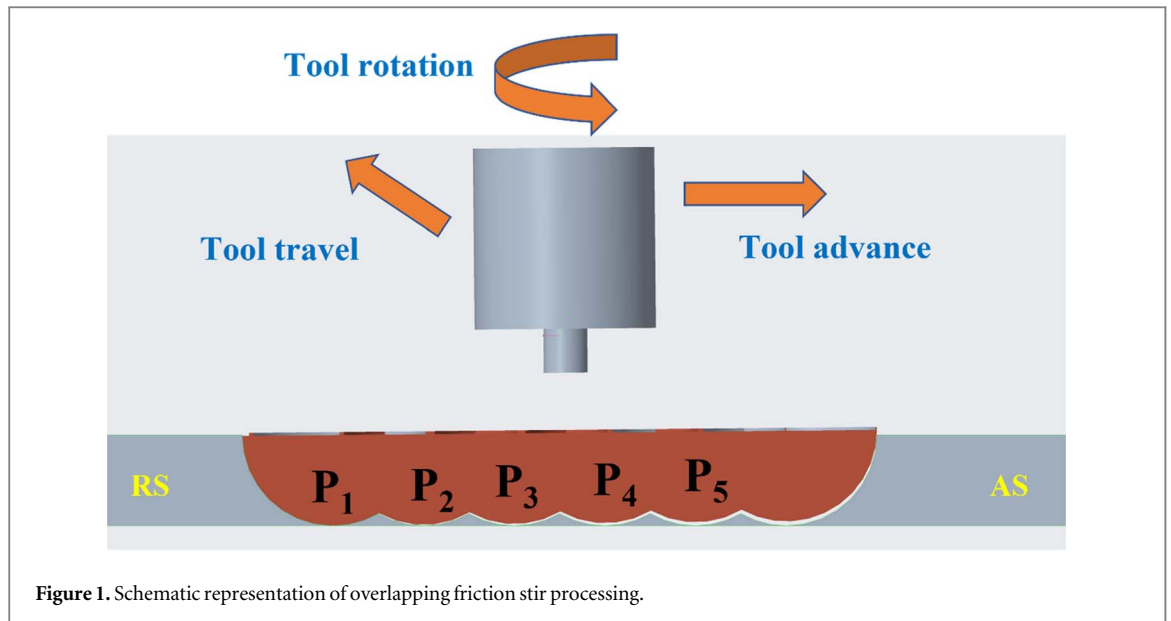


Figure 1. Schematic representation of overlapping friction stir processing.

order to overcome that problem, various authors conducted FSW in different cooling environments, such as compressed air [6], water [7], solid CO₂ [8], and liquid N₂ [5]. Some of these cooling media can be used for post-process cooling, and others can be used for in-process cooling.

The post-process cooling FSP (PP-FSP) uses solid CO₂ or dry ice as a cooling media, and the in-process cooling FSP (IP-FSP) uses water and liquid N₂ as a cooling media. Su *et al* [9] claimed that FSP produces an ultrafine-grained structure by quenching the processed region with a solution of solid CO₂, water, and methanol just after the tool travel in Al7075 alloys. According to Sinhmar *et al* [10] investigation of the microstructure and mechanical characteristics in FSW of Al2014, a recrystallized equiaxed, fine grain structure having the best mechanical characteristics, has been produced by water cooling. Additionally, it was shown that water cooling enhances mechanical qualities. To investigate the impact of quenching rate on characteristics, Kumar *et al* [11] performed friction stir welding on a 2XXX series alloy in a water and cryogenic atmosphere. It has been claimed that water-cooling friction stir welding increased strength and ductility compared to other media. The latest research by Wang *et al* [12] examined how several cooling techniques (air, water, and solid CO₂) affected the friction stir process of Al2014 alloy and discovered that FSP with solid CO₂ as a cooling media produced the best grain refining and mechanical qualities than other cooling environments. The underwater FSP on Al2219 was carried out by Feng *et al* [13] to assess the microstructural features. They attained an ultrafine-grained structure and noticed that water cooling caused a slight reduction in grain size in the stir region. For more significant grain refining, Chen *et al* [14] used the 3-pass friction stir processing on Al-Mg alloy. The findings showed that grain size is determined by rotational rate and increases with increasing rotational rate. From the FSP/FSW studies on the cooling media aspects, it was identified that in some studies, the post-process cooling FSP yielded better properties than in-process cooling FSP and vice-versa.

From the literature sources of the FSP, it was identified that most researchers concentrated on single- or multi-pass friction stir processing with 100 percent pin overlap. But the surface modified with single- or multi-pass friction stir processing with 100 percent pin overlap is not used in real-world applications because FSP with 100 percent overlapping creates a stir region of size not more than 12 mm due to the limited capacity of the FSW machine. In order to overcome that drawback, a few authors created a wide-area stir zone (WSZ) using multi-pass overlapping FSP (OL-FSP) with pin overlap. In this, after the successful fabrication of one pass, the FSP tool is moved towards the left or right side to a distance not higher than pin size and finishes the second pass, and this process will be repeated till the required numbers passes are achieved (as shown in figure 1).

A few articles exist on multi-pass OL-FSP, despite most studies on single-pass friction stir processing. In order to achieve morphological homogenization in the processing regions, overlap percentage, number of paths, and overlap directions are essential variables. Ramesh *et al* [15] carried out a 12-pass friction stir processing using a 50 percent pin overlapping on Al5086 alloy using two different techniques. The results of two FSP techniques, intermittent multi-pass friction stir processing (IM-FSP) and continual multi-pass friction stir processing (CM-FSP), showed that specimens treated with IM-FSP had superior characteristics to those treated with CM-FSP. Su *et al* [9] conducted a 4-pass OL-FSP on Al7075 alloy with a 33.3 percent pin overlapping, and the outcomes were contrasted to those of a one-pass friction stir processing. It was discovered that OL-FSP produced better results than one-pass FSP, and it was also found that this technique can be used to create thinner

Table 1. Elemental composition of Al5083.

Component	Al	Mg	Si	Cr	Cu	Fe	Mn	Ti	Zn	others
Wt%	Primary	4.07	0.12	0.07	0.06	0.23	0.55	0.01	0.111	0.15

sheets of any thickness with an ultrafine-grained morphology. Johanes *et al* [16] produced a wider area stir region in 7075 aluminum with 40 percent pin overlap among successive tracks and found that OL-FSP had a somewhat lesser ductility than one-pass FSP. Mirinda *et al* [17] looked into the impact of overlap direction by the retreating side (RS) and advancing side (AS). They stated that OL-FSP towards the advancing side produces an uneven surface quality with consistent microhardness across the homogenized stir zone, making OL-FSP a promising approach to improve mechanical qualities. According to Khaled *et al* [18], varied overlap ratios had no impact on grain refinement in the processed zone. They looked at the effects of overlapping percentages, including 25%, 50%, and 75%, on morphology, texture, and mechanical characteristics. Nevertheless, it was also observed that the material's hardness and strength decreased due to the reinforcing precipitate particles dissolving as the overlapping percent increased. Kwon *et al* [19] study of 4-pass OL-FSP on AA1050 alloy, recrystallized grain structure growth in the bulk-area treated region via FSP allowed for an increase in the mechanical characteristics. Along with the above-mentioned studies, other researchers also conducted the overlapping FSP on other alloys [20–22].

From the limited literature studies on OL-FSP, it was found that no studies focused on the impact of cooling media on the microstructure, mechanical properties, and corrosion aspects of wide-area processing zone fabricated by OL-FSP. Moreover, as per the author's knowledge, no study was conducted to compare the effect of in-process and post-process cooling on OL-FSP samples. Hence, the present study aimed to investigate the influence of post-process and in-process cooling on microstructure, mechanical behavior, and electrochemical nature of wide-area stir zone fabricated by overlapping FSP.

2. Materials and methods

2.1. Processing

In the present study, commercial Al5083-H111 plates with a size of 240 mm × 100 mm × 6 mm were utilized as the base alloy, and table 1 documents the compositional weight percentages of different alloying elements present in the base alloy. A 3-Ton capacity dedicated FSW machine was employed for creating a bulk-area processed region in the base alloy. The process variable, such as tool revolution speed of 900 rpm, travel speed of 50 mm min⁻¹, plunge depth of 0.2 mm, and tool tilt angle of 2°, was optimized from the trial experiments. The OL-FSP was performed with non-consumed tool steel with cylindrical threaded pin geometry having a shoulder diameter of 24 mm, pin length of 5.6 mm, and pin diameter of 6 mm. The wide-area stir region was processed with a 5-pass overlapping FSP with a 50 percent pin overlapping between the two successive passes (i.e., after the successful completion of each FSP pass, the tool advances towards either advancing or retreating side to a distance of 3 mm and process the next pass). The literature sources identified that the advancing side of the FSP sample is weaker than the retreating side of the FSP sample [17, 23]. Hence, the OL-FSP was carried out toward the advancing side. The schematic illustration of the OL-FSP is displayed in figure 1, where P₁, P₂, P₃, P₄, and P₅ are overlapping passes.

The authors conducted overlapping FSP with solid CO₂ as post-process cooling media and water as in-process cooling media, as displayed in figure 2. FSP was carried under two different conditions with the aid of cooling media to restrict grain coarsening and achieve further grain refinement. In the initial condition, a post-process cooling FSP (PP-FSP) has been performed with solid CO₂ as a cooling media. In this, the solid CO₂ was supplied quickly to the processed region after the tool leaves the stirring material, as shown in figure 2(a). In the later condition, water cooling or in-processing cooling FSP (IP-FSP) has been performed in submerged condition. In IP-FSP, a setup has been fabricated and kept on the table of friction stir welding equipment, as displayed in figure 2(b).

2.2. Microstructure

The specimens for microstructural examination have been cut orthogonal to the processing direction of the required sizes. The samples have been mounted in a hydraulic mounting press using Bakelite powder for easy handling. The mounted samples were then polished using various grades of SiC papers (i.e., 180, 400, 800, 1000, 1500, and 2000 grit sizes) to obtain a mirror-like finish on the sample surface, followed by cloth polishing using velvet cloth. After polishing, the samples have been cleaned with a water jet to remove the contaminants and dirt on the polishing area. The cleaned samples have been dipped in a Kellers' etchant for 140 s to acquire the desired

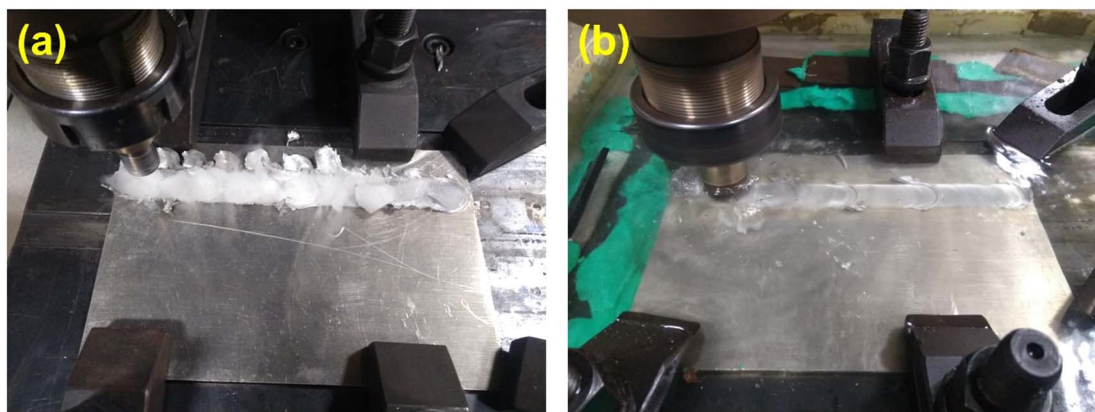


Figure 2. (a) Post-cooling FSP with solid CO₂ as a cooling media and (b) In-process cooling FSP with water as cooling media.

morphological features. After etching, the samples were kept under fully-opened tap water to wash out the etchant present on the aluminum matrix. The samples were examined with optical 3D microscopy (Maker: Metco, India Model: HRG 500) and Scanning Electron Microscopy (Maker: Tescon, Czech Republic, Model: Vegas-3) equipped with energy dispersion spectroscopy (EDS) to reveal the morphological aspects like grains and intermetallic particle dispersion in both the processed alloys.

2.3. Mechanical properties

The microhardness of the processed samples was computed using Vicker's microhardness tester (Maker: Metco, India, Model: Economet). The hardness of the specimens has been measured at 2.5 mm from the upper region and along the 24 mm length of the orthogonal cross-section with a 0.5 mm interval among the successive indentations and 100 g force to analyze the microhardness trend with a dwelling period of 15 s. Samples attaining the ASTM-E8 standards have been utilized to measure the tensile properties. The tensile samples were extracted from the bulk-area processed region along the FSP direction. Using a 100 kN universal testing machine (Maker: Instron, USA, Model: 300LX), the tension tests have been carried out in computer-controlled mode with a 10^{-3} strain rate at ambient conditions. The scanning electron microscope was utilized to study the fracture features of the tensile specimens. For each FSP condition, tension tests were performed on three specimens to get accurate results.

2.4. Electrochemical behavior

The electrochemical studies were performed on the upper surface of the processed samples employing an electrochemical workstation (Maker: CH instruments, USA, Model: 604-e). The workstation contains open circuit potential (OCP) and Tafel polarization experiments. The OCP study was performed to guarantee the potential ranges for the Tafel polarization study. The electrochemical studies were performed in the electrolyte containing 3.5 percent NaCl and 96.5 percent aerated water. The electrolytic solution attacks the processed samples of the 10 mm diameter through a hole made in the workstation, and the leftover surface was kept unexposed. Corrosion studies were performed with the 3-electrode system with the platinum electrode as the auxiliary electrode, the saturated calomel electrode as the reference electrode, and the test sample as the working electrode. The Tafel polarization test was performed at a scan speed of $0.166\text{E-}3 \text{ mV S}^{-1}$. The corroded specimens have been then examined with an optical microscopy to study the corrosion attack.

3. Results and discussion

3.1. Optical microscope

Figure 3 displays low-magnification macrostructures of the OL-FSP samples indicated with different zones. Optimized selection of processing conditions and overlap percentage led to good structural features, defect-free structure, and uniform processing area throughout the wide-area stir region. Since the overlap was done in the direction of the AS, it eliminated the flashes and irregularities formed on the AS, leading to the homogeneous flow of material in the stir regions [24].

The optical microscopic image of the Al5083 base alloy is shown in figure 4. It consists of heavily deformed coarse grains with a mean grain size of ~ 82 microns. It was also found from figure 4 that grains are oriented toward the cold-rolling direction. After friction stir processing, the heavily deformed grains in the base alloy was

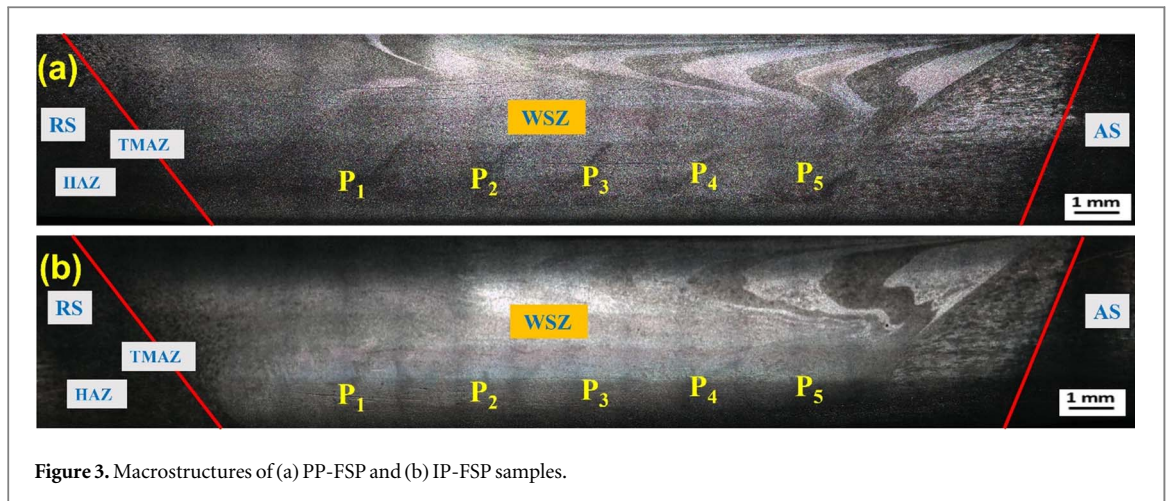


Figure 3. Macrostructures of (a) PP-FSP and (b) IP-FSP samples.

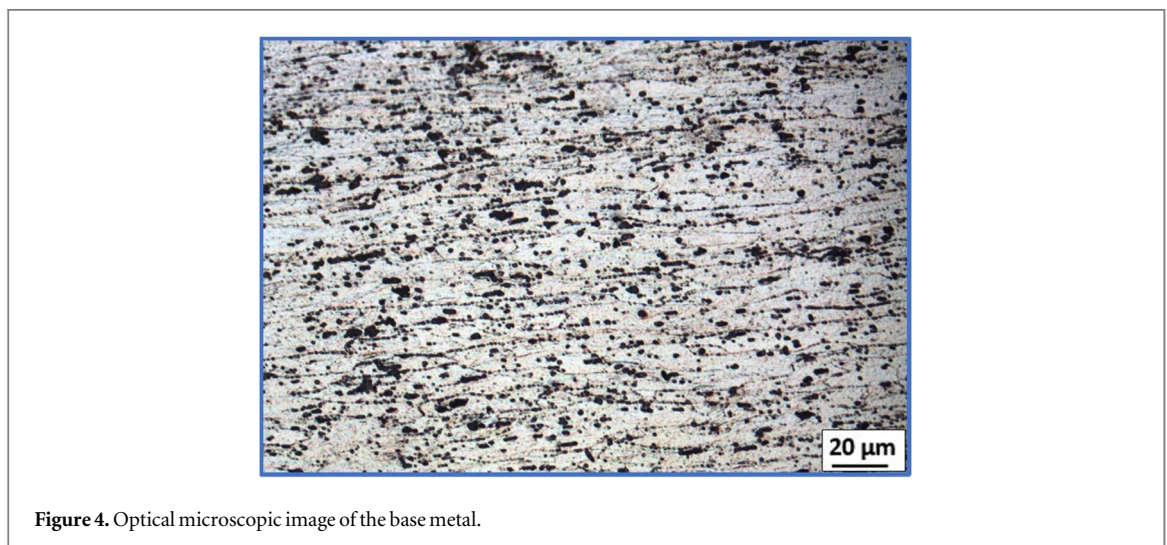


Figure 4. Optical microscopic image of the base metal.

wholly destroyed by the tool stirring action and transformed into the recrystallized equiaxed fine-grained structure with high-angle boundaries due to the intense plastic straining and thermal annealing (as shown in figures 5 and 6). It is well-known that thermal annealing of cold working material (as-received condition of base alloy) can be done in three stages: dynamic recovery, recrystallization, and grain growth. During dynamic recovery, the characteristics of the base alloy are not changed. But whatever defects are formed during or before the cold working are eliminated in the dynamic recovery process. The dislocations of the opposite sign come together, collide, and destroy themselves. But, the dislocations of the same are not destroyed, and in turn, they will act as a driving force for the nucleation of grain refinement. When the critical fine grain size is achieved, dynamic recrystallization comes into the picture and turns the grains from low-angle to high-angle boundaries. Once the tool leaves the stirring region, the frictional heat produced in the stir region causes the grain growth of refined grain structure. Thus, in order to avoid the grain growth of the refined grain structure, different cooling techniques were used in the present study. From the microstructures of OL-FSP samples in figures 5 and 6, it was identified that the IP-FSP resulted in better grain refinement than the PP-FSP sample. It is well-acknowledged that the cryogenic media (i.e., solid CO_2) produced a better cooling effect than the water as cooling media. The better grain refinement in water-cooling FSP (i.e., IP-FSP) is due to uniform heat dispersion from the processing zone by the principle of convectional heat transfer owing to the complete immersion in the water media. However, in PP-FSP, solid CO_2 influences the processing region only, while the heat from other regions of the work metal is transferred to the processed area, resulting in little grain growth compared to IP-FSP [11].

The micrographs of the stir zone in each overlapping pass (mentioned as P_1 , P_2 , P_3 , P_4 , and P_5 in figure 1) of the OL-FSP sample are shown in figures 5 and 6. Initially, the mean grain size was calculated at the center of the stir region for all overlapping passes of the OL-FSP samples using the line-intercept method. From the grain size analysis, it has been confirmed that the recrystallization is homogeneous in all passes of OL-FSP samples in both PP-FSP and IP-FSP cases. Thus, it was observed that the conduction of FSP in the successive overlapping path does not affect the grain refinement in the overlapping passes in PP-FSP and IP-FSP cases. The average grain size

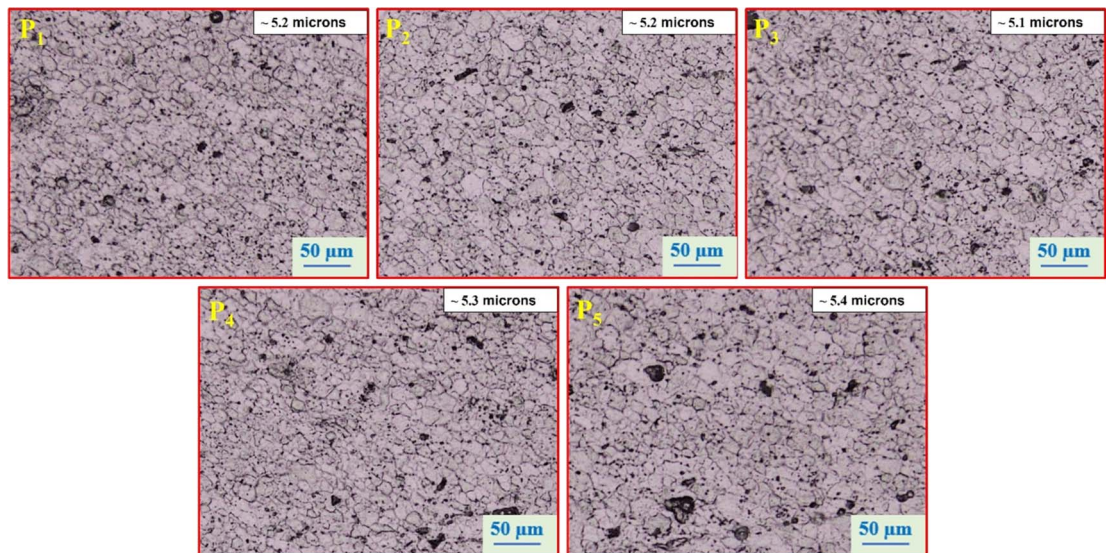


Figure 5. Optical microscopic images of overlapping stir zones in the PP-FSP sample from the first to the fifth pass indicated with grain size (in inset).

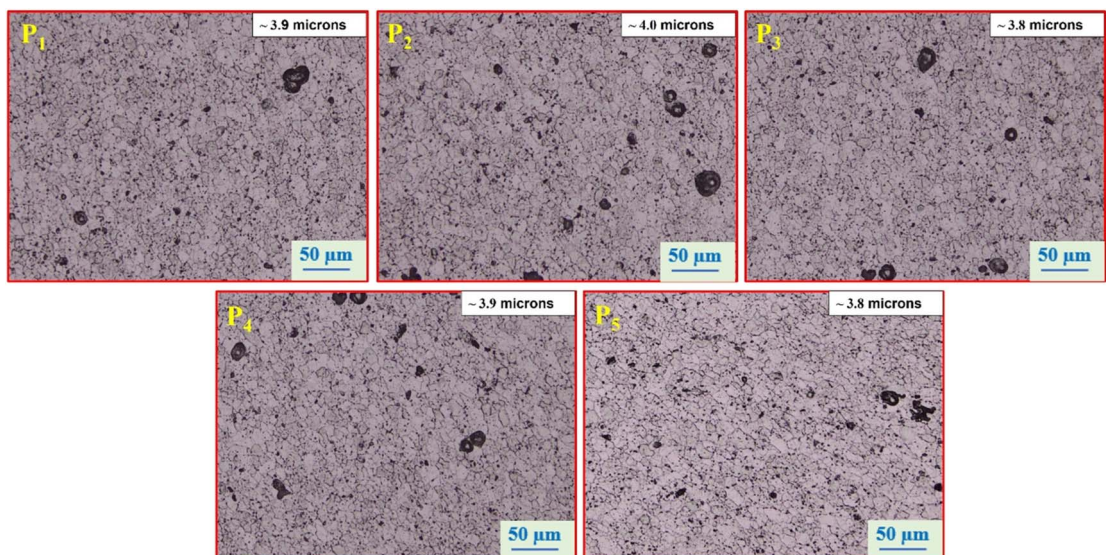


Figure 6. Optical microscopic images of overlapping stir zones in the IP-FSP sample from the first to the fifth pass indicated with grain size (in inset).

in the WSZ of PP-FSP and IP-FSP samples was computed to be ~ 5.2 and ~ 3.9 microns. The cooling media controls the grain coarsening during FSP. But, the complete removal of the heat input caused by the tool stirring action is not possible by any cooling media, as per the author's knowledge. If the complete removal of the heat input is possible by any cooling media, such cooling media is not preferred because the sufficient plastic deformation is not achieved by the mechanical and thermal action of the tool.

Later, the grain refinement was observed at the top and bottom of the wide-area stir region for both PP-FSP and IP-FSP cases, as shown in figure 7. From figure 7, it was identified that the grain size slightly differed from upper to lower region due to variations in heat generation. The grain refinement in the top region (figure 7(a) and (b)) was observed to have a coarse-grained structure compared to the grain size in the bottom region of the stir zone. At the top stir zone, the recrystallization is owing to the rotating motion of both the shoulder and probe (primary by the shoulder and partly by the pin) of the FSP tool. As per the equation $V_1 = W_a \cdot (D/2)$, (where V_1 is the linear velocity of the tool, W_a is the angular velocity of the tool or RPM of the tool, and D is the diameter of the tool at the pin/shoulder) the top stir zone produces greater heat ($\sim 70\%$) due to bigger diameter of the shoulder as compared to the smaller diameter of the pin [13, 25]. Xu *et al* [13] The investigation concluded that

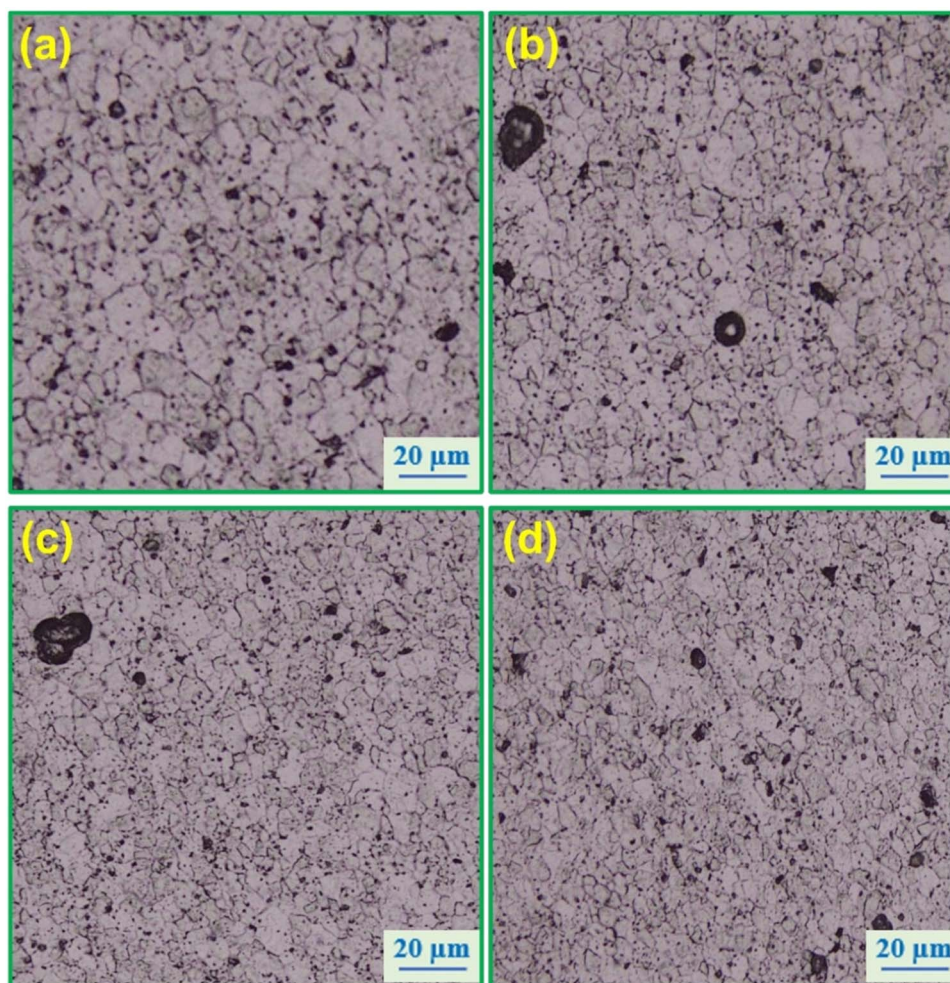


Figure 7. Optical microscopic images of the top stir region of (a) PP-FSP and (b) IP-FSP samples and bottom stir region of (c) PP-FSP and (d) IP-FSP samples.

the top stir zone is subjected to high-temperature thermal cycles for longer owing to the shoulder influence. Thus, the top stir region has a coarse-grained structure than the bottom stir regions. At the bottom stir zone (figures 7(c) and (d)), the refinement causes only by the rotating and linear action of the pin. As the pin diameter is smaller than the shoulder diameter, the shorter thermal cycles are obtained by the reduced liner velocity at the pin area, resulting in the fine-grained structure in the bottom stir region compared to the top stir zone. Also, the more swirling motion at the end of the tool also results in better grain refinement in the bottom stir region.

3.2. Scanning electron microscopy

The scanning electron microimages of stir zones of OL-FSP samples along the base alloy are depicted in figures 8 and 9. The micrograph of the base alloy includes dark regions of the alpha-aluminum matrix encompassed by intermetallics (IMs) with an average size of $\sim 1.60 \mu\text{m}$ (as shown in figure 8). However, the rotating motion of the FSP tool leads to the breaking of IMs into homogeneous fine IMs with an average size of $\sim 1.1 \mu\text{m}$ and $\sim 1.0 \mu\text{m}$ after PP-FSP and IP-FSP, as shown in figure 9. Due to the rapid cooling effect supplied in the IP-FSP specimen, the intermetallic dissolution was controlled, and the stirring motion of the tool broke the intermetallics into very fine particles. The IMs in the base alloy and OL-FSP samples were obtained in 2 different shapes: lath-shape and rod-shape. In the base alloy, the sizes of the lath-shape are more than rod-shaped IMs, whereas, in the OL-FSP samples, the lath-shape IMs are finer than rod-shaped IMs. Additionally, the number of lath-shape IMs decreased after OL-FSP. The variations in the presence of IMs in the micrographs of OL-FSP samples are owing to severe plastic deformation and thermal cycling.

EDS was performed on the IMs of the base alloy and the PP-FSP samples (as displayed in figures 8 and 9(a)). From the EDS investigation, it has been confirmed that the IMs in lath shape are iron-containing IMs (pointed as 1), while the IMs in rod shape are magnesium-containing IMs (pointed as 2), and it is attributed to the existence of various alloys and as-supplied condition (i.e., cold-rolling condition) of the base alloy. Along with the above-mentioned IMs, the continuous network of very small IMs has been identified in the grain boundary (GB) in the

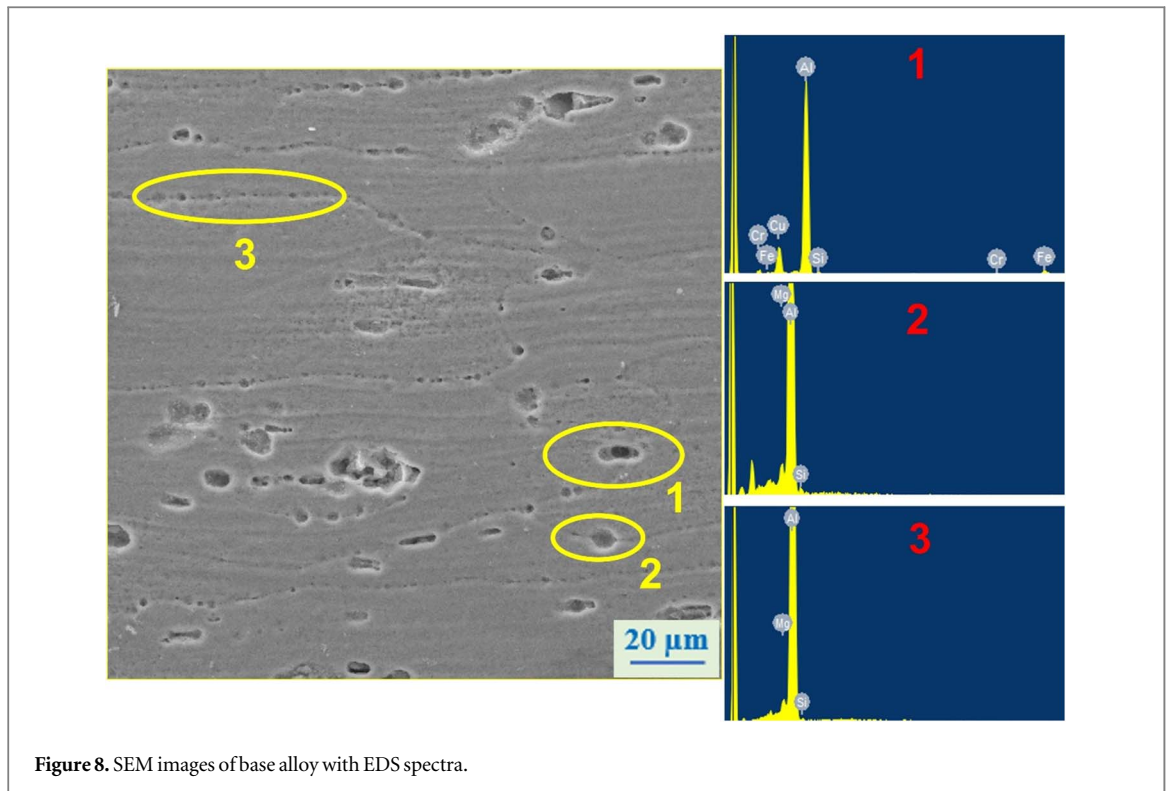


Figure 8. SEM images of base alloy with EDS spectra.

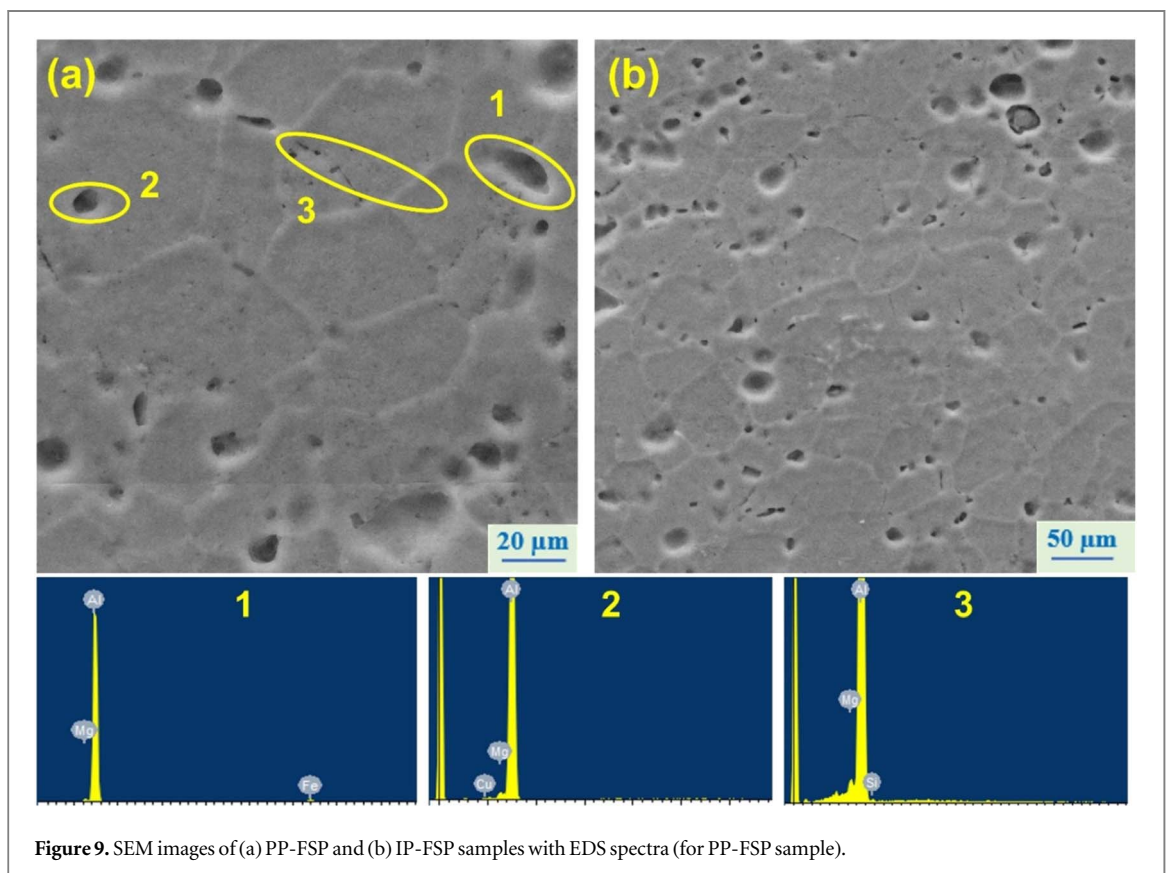
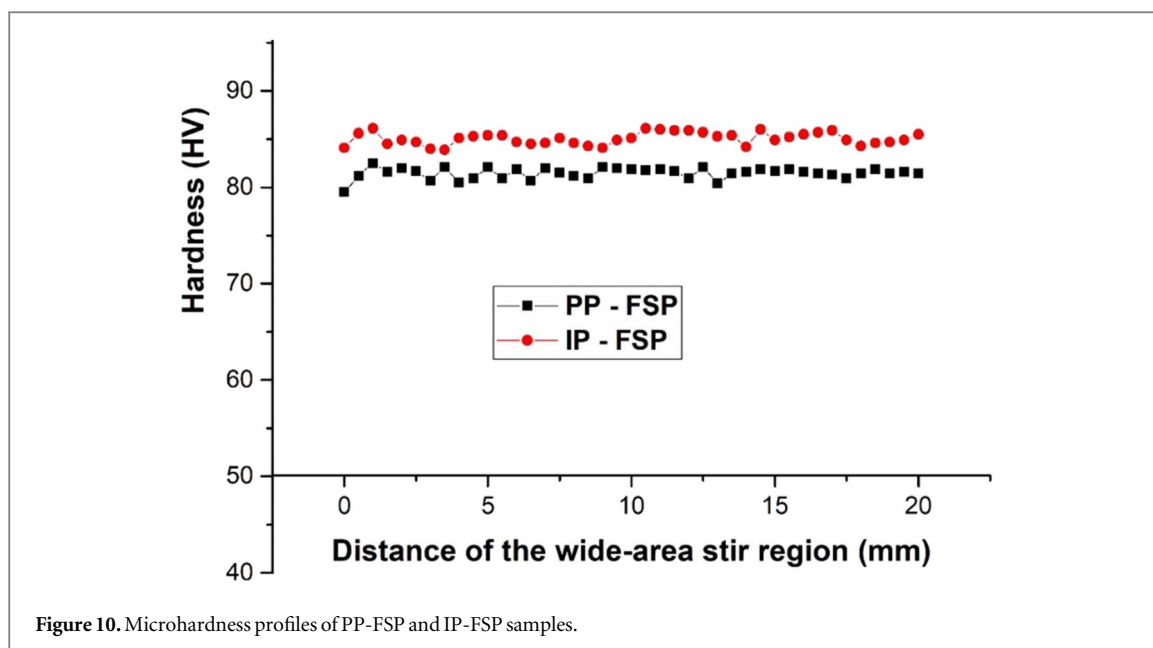


Figure 9. SEM images of (a) PP-FSP and (b) IP-FSP samples with EDS spectra (for PP-FSP sample).

base alloy, and those GB IMs have also been confirmed as magnesium-containing IMs from EDS examinations (pointed as 3). The IMs in GB hinder the migration of GBs during the tensile deformation and increase the strength.

The scanning electron micrographs of the OL-FSP specimens are depicted in figure 9. Like base alloy, the OL-FSP specimens also include lath shape IMs (i.e., iron-containing IMs) and rod shape IMs (i.e., magnesium-



containing IMs). Unlike base alloy, a discontinued chain of very small IMs has been observed in GB, and these have also been categorized as magnesium-containing IMs. The quantity of IMs is less in the OL-FSP specimen than in the base alloy. The elevated temperature cycling during the FSP led to the dissolving of IMs and resulted in less density. The quantity of magnesium-containing IMs increased after OL-FSP. After OL-FSP, the IMs were fragmented, and a small concentration of magnesium settled on existing IMs as a result of the rotating action of the FSP tool in the stir zone.

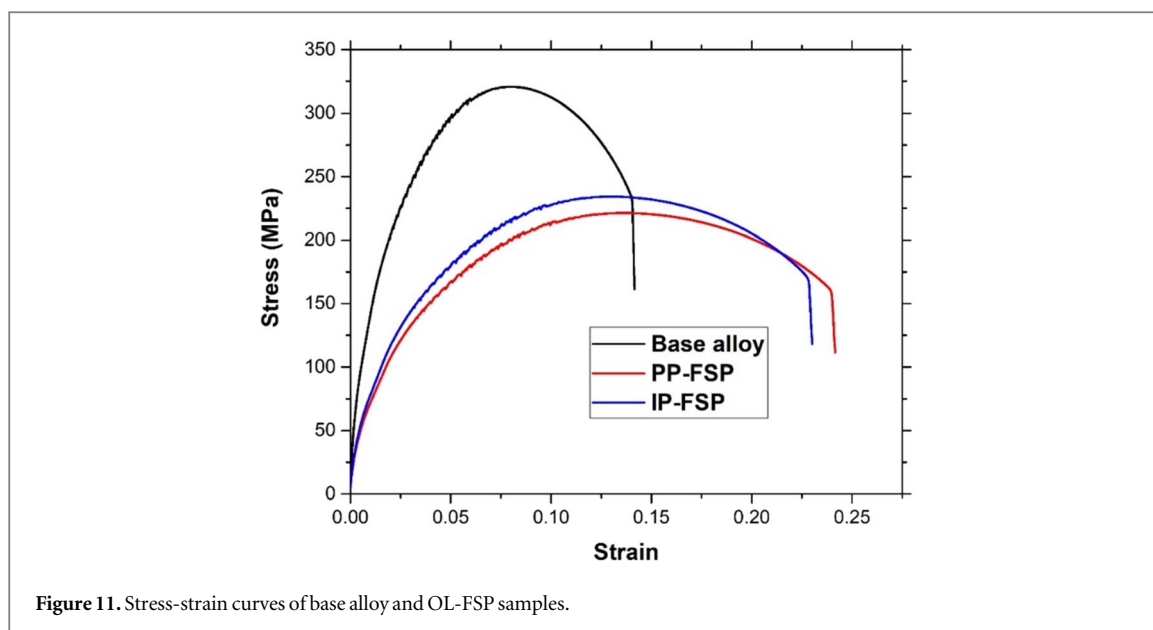
It is commonly acknowledged that the IMs control the mechanical and corrosion behavior of the base alloy and OL-FSP specimens. Initially, as compared to OL-FSP samples, the base alloy contains a high density of lath shape IMs, and these IMs serve as stress concentration regions during the tension testing, leading to abnormal failure and less elongation than the OL-FSP samples. Moreover, the lath shape IMs have an excellent ability to hinder the mobility of grain boundaries at the time of tensile and localized deformations (the indentation in the hardness test results in localized deformation) [7]. Hence, the base alloy's high density of lath shape IMs results in improved hardness and strength than the OL-FSP specimens. Secondly, the alloy additions in the IMs impact the corrosion behavior. Compared to discontinued IMs in the GB in the OL-FSP specimen, the continual network of grain boundary IMs in the base alloy can quickly form the galvanizing with the Al matrix. Based on the experiments of Gharavi *et al* [26], it has been identified that the galvanizing is formed among the iron-containing IMs (i.e., lath shape IMs) and the Al matrix. In the present examination, the density of lath shape IMs is higher in the base alloy than in OL-FSP samples, leading to quick galvanizing in the BM. Within the OL-FSP specimens, the IP-FSP sample has a fine and lower density of iron-containing IMs than the PP-FSP sample.

3.3. Microhardness

The microhardness variations across the middle section of the OL-FSP samples are shown in figure 10. It was identified from the hardness profile that hardness is approximately the same in all overlapping passes of the wide-area stir region of both IP-FSP and PP-FSP samples, and it was concluded that the overlapping FSP did not lead to variations of hardness in the wide-area stir region due to fact that the homogeneous grain refinement in each overlapping pass. It has been observed that the OL-FSP specimens exhibited reduced microhardness in the stir zone as compared to the base alloy (94 ± 12 HV). The raw material (i.e., base alloy) was supplied in cold-rolling conditions, which experiences a work-hardening effect, contributing to enhanced hardness. Also, the stir region experiences elevated thermal cycles, which softens the processed region and lowers the hardness in the stir region [14]. Zhao *et al* [27] investigations reported that the reduction in the density of lath shape IMs in the stir region of Al-Mg-Si processed by FSP resulted in a significant drop in hardness than the base material. The uniform hardness in the wide-area stir regions of PP-FSP and IP-FSP samples is 81 ± 5 HV and 85 ± 6 HV. The factors for hardness reduction in the PP-FSP sample are explained tensile characteristics section.

3.4. Tensile characteristics

In order to examine the influence of OL-FSP, tensile characteristics such as yield strength (YS, MPa), ultimate tensile strength (UTS, MPa), and ductility (EL, %) of the OL-FSP samples were contrasted with the base alloy. Table 2 displays the tensile characteristics of the base alloy and OL-FSP samples calculated from the stress-strain

**Table 2.** Tensile data.

Sample	Ultimate tensile strength (MPa)	Yield strength (MPa)	Ductility (%)	Strain hardening parameter (MPa%)
BM	321±6	241±5	14±2	4494
PP-FSP	221±5	142±3	24±3	5304
IP-FSP	232±5	150±3	23±4	5336

plots (as shown in figure 11). The tensile data clearly showed that the strength of OL-FSP specimens was inferior to that of the base alloy due to thermal annealing during multi-pass overlapping friction stir processing, as reported in the microhardness investigation. Khaled *et al* [18], investigations reported that the drop in UTS and microhardness in the FSPed specimens is owing to the dissolution of intermetallic particles and limited re-intermetallic formation. However, the OL-FSP resulted in ductility improvement of about 178 percent and 175 percent of base alloy in PP-FSP and IP-FSP samples. The enhancement in ductility could be due to the uniform strain distribution, which supports deformation to be homogeneous in a longitudinal tensile specimen extracted from the large-area stir region. As per the studies Chen *et al* [14], the enhancement in processing specimen ductility is owing to the homogenous fine-grained structure and less dislocation density of the FSPed specimen. Moreover, the density reduction of the lath shape IMs in OL-FSP samples led to ductility enhancement.

Within the OL-FSP specimens, the IP-FSP resulted in greater strength and hardness and less ductility than PP-FSP samples due to the fine-grained structure, fine IMs, and less density of needle shape IMs. In many industrial sectors and aerospace applications, the term strain hardening parameter (i.e., the product of strength (UTS) and ductility (EL)) is being used to assess the comprehensive effect of strength and elongation [7, 14]. As reported in table 2, the more excellent strain hardening parameter value was obtained for the OL-FSP samples, and within the OL-FSP samples, the best strain hardening parameter was obtained for IP-FSP samples, which will be more useful in practical applications.

Fracture features of the base alloy and OL-FSP tensile specimens were investigated using a scanning electron microscope, as shown in figure 12. The fracture morphology of the base alloy contains a high density of deep dimples, considered a pure ductile fracture, as shown in figure 12(a). Compared to base alloy, the quantity, and size of the dimples are decreased in OL-FSP specimens due to the presence of refined grain structure and material flow during FSP. The fractures were developed in 45° for OL-FSP samples. In both OL-FSP samples, the dimples were replaced by the flat regions. Finally, the fracture features of both samples have a mixture of dimples and flat regions, and this kind of fracture was considered a brittle-ductile fracture. The density and size of the dimples were further decreased and replaced by the flat region in IP-FSP samples due to the rapid cooling effect (figures 12(b) and (c)).

3.5. Electrochemical behavior

Tafel plots acquired from the electrochemical investigation are displayed in figure 13, and corrosion potential (E_{CORR}) of base alloy and OL-FSP specimens were calculated from the Tafel plots listed in table 3. It is commonly

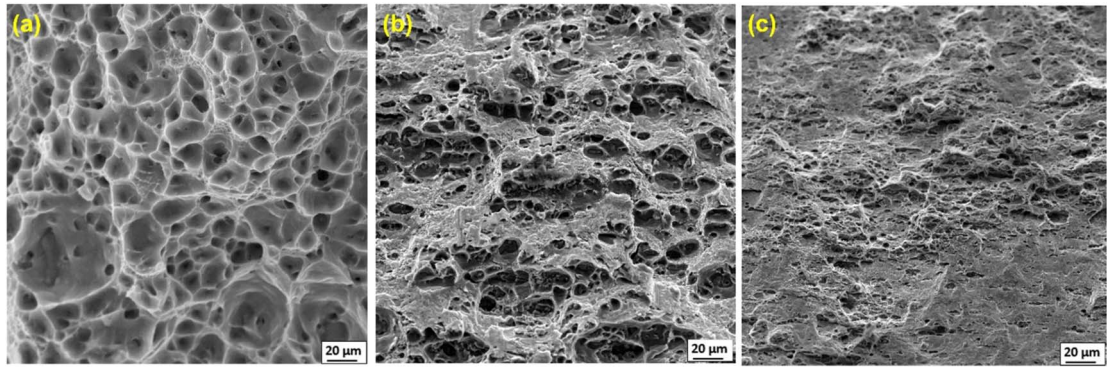


Figure 12. Fracture images (a) base alloy, (b) PP-FSP, and (c) IP-FSP samples.

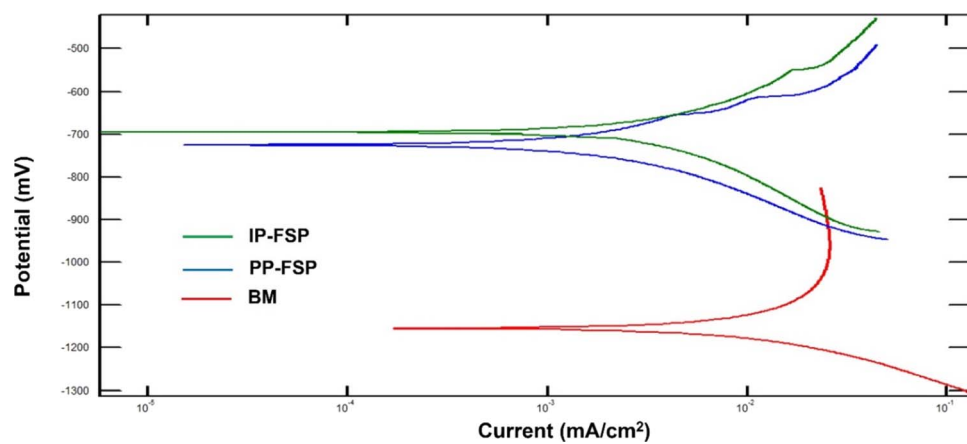


Figure 13. Tafel curves of base alloy and OL-FSP samples.

Table 3. Corrosion potential values.

Sample name	Base alloy	PP-FSP	IP-FSP
E_{CORR} (mV)	-1161	-720	-690

acknowledged that the greatest negative E_{CORR} indicates less corrosion resistance, whereas less negative E_{CORR} indicates more excellent corrosion resistance. It has been concluded from Tafel tests that the E_{CORR} of base alloy exhibited a higher negative value than the E_{CORR} of OL-FSP specimens, which proved that the corrosion resistance greatly enhanced after friction stir processing.

Generally, corrosion happens because of the potential variance between cathodic and anodic elements, and lesser potential variance indicates more excellent resistance to electrochemical activity. During the electrochemical activity, the anodic element (higher negative E_{CORR}) is more prone to electrochemical activity where an anodic reaction happens. On the other hand, the cathodic element (lesser negative E_{CORR}) is less prone to electrochemical activity where a cathodic reaction happens. The general electrochemical reactions of aluminum in the electrolyte are as follows [13, 25].

Anodic reaction:



Cathodic or reaction:



In the process of Tafel testing, the cathodic reaction induces the evolution of hydrogen observed on the surface of the cathodic element. The cathodic reaction leads to aluminum surface dissolution since it functions as an anodic element concerning adjacent intermetallic particles. In the current investigation, the aluminum



Figure 14. Corroded images (a) base alloy, (b) PP-FSP, and (c) IP-FSP samples.

matrix serves as an anodic element, and the intermetallics close to and within grain boundaries serve as a cathodic element. As stated in the previous analysis, the E_{CORR} of the cathodic element is greater than the anodic element; hence, it dissolves and corrodes the aluminum matrix encompassed by IMs. The galvanizing is formed between the aluminum matrix and IMs in the grain boundaries due to their potential differences. Figures 8 and 9 (SEM micrographs provided with EDS spectrum) indicates that the base alloy contains a more significant number of IMs and a continual network of IMs in the grain boundaries. On the other hand, the OL-FSP specimens contain less number of IMs and discontinued IMs in the grain boundaries. The galvanization between the coarser IMs and the aluminum matrix in base alloy leads to more significant potential variation than in the galvanization between the small IMs and aluminum matrix [28]. Factors such as discontinued IMs in the grain boundary and a more significant potential variation in the base alloy led to the specimens becoming more prone to electrochemical activity. On the other hand, the recrystallized small grains in OL-FSP specimens can form an oxide layer better than coarser grains in the base alloy. The oxide layer serves as a protective film and restricts the electrochemical activity [29]. So, OL-FSP specimens are more excellent and resistant to electrochemical activity than base alloy. Owing to the existence of very small grains, the specimen processed with water cooling media led to a more excellent corrosion-resistant specimen than the sample processed with solid CO_2 as a cooling media. Finally, the Tafel studies' outcomes coincide with the microstructural analysis. In the base alloy, severe electrochemical activity was identified as larger pits (figure 14(a)). The electrochemical activity decreased after the PP-FSP (figure 14(b)) and decreased further after the IP-FSP (figure 14(c)), and these outcomes coincide with the Tafel test results. Moreover, the electrochemical activity of both FSP specimens is approximately homogeneous, and small pits were identified in both specimens.

4. Conclusions

A wide-area processing region was successfully fabricated using post-process and in-process cooling technologies in Al5083 alloys using OL-FSP, and the following conclusions were extracted from the findings.

1. Macrostructural findings stated that the defect-free structure was obtained in the cooling-assisted processes due to the optimum selection of process parameters, overlapping direction, and the overlapping ratio.
2. OL-FSP led to the development of refined grain structure in the wide-area stir region due to the dynamic recovery and dynamic recrystallization.
3. It has also been identified that the OL-FSP did not influence the grain size variation in the wide-area stir region, and the grain size is homogeneous throughout the large-area stir region.
4. Along with the recrystallization, the cooling environment also provided grain refining. Within the two FSP conditions, the specimen fabricated in water resulted in a small grain structure due to the rapid cooling effect.
5. Three different kinds of IMs, such as lath shape iron-contained IMs, rod shape magnesium-based-contained IMs, and very small magnesium-based-contained IMs in the grain boundaries, have been found in base alloy and both OL-FSP samples, and these IMs has a significant effect on mechanical characteristics and electrochemical behavior.
6. Due to uniform grain refinement, the hardness was found to be approximately in all overlapping passes of PP-FSP and IP-FSP samples. On the other hand, the ductility was significantly enhanced after FSP, and a better strain hardening parameter was obtained for the IP-FSP sample.

7. Electrochemical results stated that the corrosion resistance in the OL-FSP samples was greatly enhanced because of the unformed fine-grained structure and less density of iron-contained IMs.
8. Finally, it was concluded that in-process cooling technology produces a better cooling effect than post-process cooling technology. It was suggested to conduct the FSP with in-process cooling conditions rather than post-process conditions to achieve excellent properties.

Data availability statement

The data cannot be made publicly available upon publication because no suitable repository exists for hosting data in this field of study. The data that support the findings of this study are available upon reasonable request from the authors.

Funding

The authors declare that no funding was received for this work.

Conflict of interest

The article was sent for publication in the Journal. The authors have no conflicts of interest. This is the original work of the authors and has not been previously published in other publications.

ORCID iDs

B V S Keerthana  <https://orcid.org/0000-0001-9408-3166>

References

- [1] Nandan R, DebRoy T and Bhadeshia H K D H 2008 *Prog. Mater. Sci.* **53** 980–1023
- [2] Mishra R S and Ma Z Y 2005 *Materials science and engineering: R: reports* **50** 1–78
- [3] Satyanarayana M V N V, Kumar A and Kranthi Kumar K 2021 *Proc. Inst. Mech. Eng. Part L J. Mater. Des. Appl.* **235**
- [4] Charit I and Mishra R S 2018 *J. Mater. Sci. Technol.* **34** 214–8
- [5] Jacob A, Maheswari S, Noor Siddiquee A and Gangil: N 2018 *Mater. Res. Express* **5** 076518
- [6] Sharma C, Dwivedi D K and Kumar P 2012 *Mater. Sci. Eng.* **556** 479–87
- [7] Satyanarayana M V N V and Kumar A 2021 *Proceedings of the Institution of Mechanical Engineers, Part L: Journal of Materials: Design and Applications Part L: Journal of Materials: Design and Applications* vol 235, pp 2454–69
- [8] Devaraju A and Kishan V 2018 *Mater. Today Proc.* **5** 1585–90
- [9] Su J Q, Nelson T W, McNelley T R and Mishra R S 2011 *Mater. Sci. Eng. A* **528** 5458–64
- [10] Sinhmar S and Dwivedi D K 2017 *Mater. Sci. Eng.* **684** 413–22
- [11] Satyanarayana M V N V and Kumar A 2020 *Proc. Inst. Mech. Eng. Part C J. Mech. Eng. Sci.* **234** 4520–34
- [12] Wang Q, Zhao Y, Yan K and Lu S 2015 *Mater. Des.* **68** 97–103
- [13] Feng Xu W, Ma J, Wang M, Jian Lu H and Xuan Luo Y 2020 *Trans. Nonferrous Met. Soc. China (English Ed.)* **30** 1491–9
- [14] Chen Y, Ding H, Malopheyev S, Kaibyshev R, Hui Cai Z and Jing Yang W 2017 *Trans. Nonferrous Met. Soc. China (English Ed.)* **27** 789–96
- [15] Ramesh K N, Pradeep S and Pancholi V 2012 *Metall. Mater. Trans. A Phys. Metall. Mater. Sci.* **43** 4311–9
- [16] Johannes L B and Mishra R S 2007 *Mater. Sci. Eng.* **464** 255–60
- [17] Gandra J, Miranda R M and Vilaça P 2011 *Mater. Sci. Eng.* **528** 5592–9
- [18] Al-Fadhalah K J, Almazrouee A I and Aloraier A S 2014 *Mater. Des.* **53** 550–60
- [19] Kwon Y J, Shigematsu I and Saito N 2003 *Mater. Trans.* **44** 1343–50
- [20] Venkateswarlu G, Devaraju D, Davidson M J, Kotiveerachari B and Tagore G R N 2013 *Mater. Des.* **45** 480–6
- [21] Alavi Nia A, Omidvar H and Nourbakhsh S H 2014 *Mater. Des.* **58** 298–304
- [22] Xue P, Xiao B L and Ma Z Y 2013 *J. Mater. Sci. Technol.* **29** 1111–5
- [23] Satyanarayana M V N V, Adepu K and Chauhan K 2021 *Met. Mater. Int.* **27** 3563–73
- [24] Zhao H, Pan Q, Qin Q, Wu Y and Su X 2019 *Mater. Sci. Eng.* **751** 70–9
- [25] Xu W and Liu J 2009 *Corros. Sci.* **51** 2743–51
- [26] Gharavi F, Matori K A, Yunus R, Othman N K and Fadaeifard F 2016 *Trans. Nonferrous Met. Soc. China (English Ed.)* **26** 684–96
- [27] Zhao Y H, Lin S B, Wu L and Qu F X 2005 *Mater. Lett.* **59** 2948–52
- [28] Gharavi F, Matori K A, Yunus R and Othman N K 2014 *Mater. Res.* **17** 672–81
- [29] Kalita S J 2011 *Appl. Surf. Sci.* **257** 3985–97